An experimental study of the electromechanical impedance method for sensors embedded in a 3D printed plate employing capacitance as structural health sensitive feature

Malinowski, Paweł H.; Andrearczyk, Artur; Singh, Shishir Kumar

DOI
10.1016/j.measurement.2025.119460

Publication date
2026

Document Version
Final published version

Published in
Measurement: Journal of the International Measurement Confederation

Measurement 258 (2026) 119460

Contents lists available at ScienceDirect

Measurement

journal homepage: www.elsevier.com/locate/measurement

An experimental study of the electromechanical impedance method for sensors embedded in a 3D printed plate employing capacitance as structural health sensitive feature

Paweł H. Malinowski [a,*], Artur Andrearczyk [a], Shishir Kumar Singh [a,b]

[a] Institute of Fluid-Flow Machinery, Polish Academy of Sciences, 14 Fiszera Street, Gdańsk 80-231, Poland
[b] Aerospace Structures & Materials Department, Delft University of Technology, Delft 2629 HS, the Netherlands

ARTICLE INFO

Keywords:
Electromechanical impedance
Damage detection
Damage identification
Additive manufacturing
3D printing
Laser vibrometer

ABSTRACT

The growth of additive manufacturing requires methods to assess the structural condition of the 3D printed structural parts. This research focuses on the electromechanical impedance method that proved its effectiveness in damage assessment of structures made of metals and fibre reinforced polymers. This work investigates a square plate with four piezoelectric sensors for EMI measurements. Three sensors were embedded in the material and one was surface bonded. The laser vibrometer was used to assess the sensors excitation range. The vibrometer study indicate high attenuation of the material and allowed us to determine that the EMI investigations should be made for frequencies up to 100 kHz. The capacitance of a piezoelectric sensor is proposed as a structural health sensitive feature. The mean value of capacitance allowed to separate the responses from individual sensors but failed to give information about the structural condition. The relation between the depth of sensor embedding and capacitance mean value was established. The work proposes a new 3-step approach for damage assessment: 1. polynomial fitting of capacitance spectra, 2. principal component analysis 3. Euclidean distance-based damage index. The approach showed sensitivity to a mass placed at three distances from the sensors and to the through thickness drilled hole of four diameters. The results indicated that the structural damage assessment can be realized in a relatively low frequency range (below 100 kHz). Structural health assessment using electromechanical impedance can be realized by embedded sensors but their sensitivity is lower than for the surface bonded sensor.

1. Introduction

Additive manufacturing (AM), or 3D printing, has become a very popular manufacturing approach. It allows for obtaining complex shapes of structural elements not achievable previously for traditional manufacturing methods. Moreover, it is environmentally friendly due to reduction of waste allowed by the non-subtractive nature of the process. Metal, polymer, or composite parts can be manufactured in this way [1]. Similarly, as for the structures traditionally manufactured, there is a need for nondestructive evaluation (NDE) or structural health monitoring (SHM) of the 3D printed structures. This requires the development of accurate and reliable methods for evaluating and monitoring the structural integrity of such components. Ultrasound-based approaches are among the techniques under intensive investigation. The resonant ultrasound spectroscopy was used to estimate the elastic properties of the manufactured material and the amount of lack-of-fusion porosities [2]. In [3] authors were able to identify the infill density of acrylonitrile butadiene styrene (ABS) samples using non-destructive ultrasonic imaging. While the infill pattern type and its ratio was studied showing its influence on the vibration characteristic of the investigated beams [4]. Some of the most well know SHM methods are based on Lamb wave propagation. Researchers used a 3D-printed ultrasonic wedge to produce S0 Lamb waves for the detection of delamination during the printing process [5]. In another study, the nonlinear wave generation that follows the onset of fatigue-damage development in printed aluminum plates was investigated [6]. A monotonic increase in the nonlinear parameters was noticed with the increase in the number of fatigue cycles. In the ultrasonic-based SHM field there are also successful attempts to use printing for sensors [7]. This allowed replacement of the bonded sensors with structure-integrated sensors working up to 20 MHz.

* Corresponding author.
E-mail address: pmalinowski@imp.gda.pl (P.H. Malinowski).

https://doi.org/10.1016/j.measurement.2025.119460
Received 11 April 2025; Received in revised form 6 October 2025; Accepted 21 October 2025
Available online 25 October 2025

This research focuses on damage assessment based on the electromechanical impedance (EMI) method [8]. The method employs piezoelectric transducers that excite the investigated structure and sense the response. The damage assessment is based on collecting the electrical quantities (impedance, resistance, conductance, and others) as a function of frequency and comparing the responses at different structural conditions. In particular, the unknown case (possibly damaged) is compared with data for known healthy (undamaged) cases. The comparison is performed based on numerical metrics. One of such commonly used metrics is the root mean square deviation (RMSD) [7]. The common advantage of using such metrics is straightforward calculation, while the main disadvantage is that they compare only two spectra (unknown state vs reference). It is also often seen that the RMSD is sensitive to noise. An successful example of using smart aggregate EMI sensors for concrete and employing the RMSD index was reported in [9,10]. However, researchers indicate such metrics have some limitations in terms of damage assessment. Small damage near the sensor give similar response as larger damage farther away [11]. To cope with such problems a clustering method was introduced to group the EMI sensors with similar behaviour for reinforced concrete structures [11], as well as model updating procedure using particle swarm [12]. Recently, various studies using impedance-based techniques have been conducted to prove their applicability also on large-scale civil structures such as 2-meter long concrete beams [13], half-meter long prisms [14], multi-strand anchorage [15], and reinforced concrete (RC) cylinders monitored wirelessly [16]. In the context of additive manufactured structures the RMSD index was employed for the sensitivity study of the EMI method to damage in 3D-printed polylactic acid (PLA) plates with varying infill densities [17]. The conductance and resistance values were merged before the RMSD damage index was employed for the damage-sensitivity analysis. It was discovered that as infill density drops the damage-sensitivity distance also decreases. Meanwhile, dimensional mistakes, positional inaccuracies, and internal porosity faults were also examined by comparing baseline readings of defect-free parts [18]. The technique identified displacements in nylon and jetting VeroWhite Plus parts. In another study, the EMI was employed together with X-ray and modal analysis for 3D printed plastics [19]. The EMI indicated local stiffness losses and weak layers bonding. Apart from the index-based damage detection approaches the principal component analysis (PCA) gained researchers interest. The PCA was developed by Karl Pearson and integrated to the mathematical statistics by Harold Hotelling to reduce dimensions of multivariable complex data set [20]. PCA technique is modern data analysis method used to find patterns in the high dimensional data sets. The PCA model was employed for the EMI data in identification of loose bolts in bolted aluminium plate structure [21]. The PCA helped to reduce the amount of data to be transferred wirelessly. The kernel PCA-based data normalization technique was used to improve damage detectability under varying temperature and external loading conditions in bolt loosening of metal fitting lug which connects the aircraft wing to a fuselage [22]. Damage detection was performed using artificial neural networks whose inputs were derived from PCA of damage metrics in [23]. PCA helped to eliminate environmental changes in jacket type tidal current power plant structure [24]. The PCA served as a mean to eliminate the environmental changes. The PCA-based algorithm was used to filter out temperature effects in of pre-stressed tendon anchorages [25]. The filtering was conducted by applying the PCA on the damage indices.

The additive manufacturing allows for more freedom with respect to the designing of structural parts. So, this works explores the possibility to embed structural health monitoring sensors during the manufacturing. The comparison is performed on the sensitivity of these sensors with relation to the surface-bonded sensor. The piezoelectric sensors were embedded in a polymer 3D-printed plate. The previous work on electromechanical impedance with embedded sensors studied a polylactic acid (PLA) beam in [26]. The embedded sensor was 6.35 mm in diameter and 0.254 mm in thickness. The specimens were fabricated using fused deposition modeling (FDM). The EMI measurements were made up to 100 kHz with a large 10 kHz step. The research showed successful detection of mass loading of the cantilever beam using the RMSD index calculated for the resistance, but no other damage-like cases were studied. The piezoelectric sensor network was successfully embedded into a composite structure with purpose of guided wave and EMI-based diagnostics [27]. The sensor network was incorporated as a SMART layer and the embedding effect was observed in the resistance spectrum of the sensor. It should be stressed that EMI only-based sensor networks were also used. A single damage localization in sandwich composite panel was achieved [28], and four sensor-based triangulation was employed in aluminium plate [29]. The EMI-based localization was further developed for multiple damage localization for a 3D-printed ABS plate and a composite plate [30]. An effective approach was proposed that splits an uniform network of surface-mounted piezoelectric sensors into subnetworks. The additional mass and drilled holes in an 3D-printed ABS plate were successfully localized.

In the research reported here four sensors were used for the sample assessment. Three sensors were embedded at three different depths. The fourth sensor was surface bonded for referential purposes. Firstly, the structural change was simulated by an additional mass. Secondly, a through-thickness hole was drilled to simulate damage, and the EMI responses were compared for four diameters of this hole. The initial study indicates that the RMSD index based on resistance can differentiate the added mass cases [31] and detect the 4 mm diameter hole presence. The research reported here is much broader. This paper proposes a unified approach to differentiate the structural changes caused by additional mass and damage simulated by drilling. Before EMI studies, the effective excitability of the sensors was tested with the scanning laser Doppler vibrometer (SLDV). The full field measurement and analysis was conducted. Fakih et al. [32] observed significant influence of the varying infill density on wave propagation in a 3D-printed PLA plates. In this work the SLDV study allowed the determine the effective frequency range to be used with the EMI.

The build-in sensors can be effectively used for assessment of composite structures. In the past research it was shown that sensors supported on a thin flexible dielectric film can be integrated in a structure [27]. Successful results were obtained for complex composite structures such as automobile side frame and liquid fuel bottle. Such sensors form an network that can be used with either active sensing or passive sensing to monitor the health condition of a structure throughout its lifetime. Similarly, in other research the sensors were successfully embedded into concrete forming smart aggregate effective used for structural monitoring in civil structures [33]. In other work the EMI was applied to a test bridge made of reinforced concrete using a network of 11 piezoelectric patches. The conductance response was studied and its sensitivity to cracks caused by loading of the bridge [34]. Another work studied the configurations of piezoelectric sensor networks for the reinforced concrete. In particular, the influence of the positioning and embedding was shown. The studied cases comprised of sensors placed in grooved notches and cement paste coated to enhance the interaction with inspected structure [14]. The embedded sensors ware used for phase transitions and strength development monitoring in blended concrete systems through shifts in conductance signatures [35]. Since, more and more structural parts are 3D printed, there is a need for investigation how the built in sensors perform for inspecting them. There are four main contribution of this research. 1. A comparison of three embedded sensors with respect to and surface-bonded sensor was conducted. 2. The relation between the depth of sensor embedding and capacitance mean value was established. 3. Frequency dependent capacitance of a piezoelectric sensor was proposed as a structural health sensitive feature. 4. New data processing method was introduced that is based on polynomial fitting, principal component analysis, and Euclidean distance-based damage index. The advantage of the proposed approach lies in its simplicity. There is no need to track peak shift that change due to structural damage/modification [33]. The mean value of the frequency

dependent capacitance allowed to separate the responses from individual sensors but failed to give information about the structural condition. By further analysis the structural condition was successfully assessed by 1. employing polynomial fitting to the capacitance spectra, 2. principal component analysis (PCA), 3. employing Euclidean distance-based damage index. The another important observation from this study is that the embedded sensors are characterized by lower sensitivity than the surface-bonded sensor.

The research and results reported in this paper are organized as follows. Section 2 describes the sample preparation procedure together with the sensor embedding process. Section 3 shows the SLDV results, and is followed by the main part describing the EMI study in section 4. Section 5 summarizes the conducted research.

2. Sample preparation and sensor embedding

The investigations started with preparing the sample. A 3D printed plate with dimensions 150 mm × 150 mm × 5 mm was additively manufactured. The plate was printed from M3-X material using the multi-jet printing technique (MJP) on a ProJet 3500 HD Max machine. The MJP is characterized primarily by putting material layers through print head jets, which are distributed throughout the whole printing platform. MJP printer uses two types of materials, each of them having a different function. The first one (wax) is responsible for supporting the manufactured structure, and the second one (polymeric resin) is the building material. After the printing process, the model is subjected to a wax melting process (using an oven) and then the remaining wax layers are removed using an ultrasonic bath. UV curing of a material substantially affects printing quality as compared to curing by oxygen. There is no vaporization of the building material, so its volume does not change, which keeps the exact dimensions of a printed element. In MJP technology, a polymeric resin is employed as a building material. The material is deposited layer by layer. After putting each layer it is cured by ultraviolet (UV) light. The chosen material (M3-X) is characterized by static tensile strength (including different directions of printing) equal to 55 MPa, so if a flat plate is printed it is isotropic in-plane. The maximum operating temperature for that material is equal to 88 °C. The resolution in one of the printing axis reaches 1600 DPI which means that one layer thickness is equal to 16 μm.

In order to embed the sensors the sample was printed with three dedicated slots:

1. at a depth of 1.15 mm from the top surface to accommodate the shallow sensor,
2. at a depth of 2.15 mm from the top surface to accommodate the middle sensor,
3. at a depth of 3.15 mm from the top surface to accommodate the deepest sensor.

Each of these slot centers was located at the center of one sample edge as shown in Fig. 1. The slots were designed to accommodate a piezoelectric disc of 10 mm diameter and 0.5 mm thickness. The CeramTec piezoelectric transducers were used as sensors. They were manufactured out of the SONOX P502 material. In order to embed the sensors the slots for sensors are filled with the printing material to about the 0.15 mm level, so the sensors are located at 1, 2, and 3 mm depths from the top surface. After the sensors are placed it is covered with the additional material. The material during refilling is in full liquid phase after preheating to a temperature of 68 °C. This temperature is safe for the used sensors since the SONOX P502 Curie temperature is 335 °C [36]. The material to fill the hole was deposited with a syringe. About 5 refills were needed to fill the deepest (3.15 mm) hole. After each refill step, the material is cured using an UV lamp. The fourth sensor (surface sensor) was glued at the sample surface near the remaining free edge. The used glue was the cyanoacrylate glue – Super Glue® (https://superglue.pl/en/superglue_en//). The measured glue thickness for the surface sensor was 0.1+/-0.02 mm. The photograph of the sample with all the sensors is shown in Fig. 2. The cables soldered to the sensors were from 350 up to 450 mm long. No additional shielding or grounding was used during the measurement. Each sensor was measured individually with the impedance analyzer L2000 4-terminal probe attaching alligator clips to the wires from the sensor. The sample was laid flat supported at the edges during EMI measurements.

The embedding of the sensors was verified by the ultrasonic B-scans performed with the Eddify GEKKO flaw detector employing a 5 MHz 64 elements phased array head without a wedge. The inspection was made from the other surface of the plate so the surface-bonded sensor is visible at the bottom in this imaging (Fig. 3d). This sensor and the shallowly embedded sensor (Fig. 3c) were the easiest to visualize. The echo from the sensor embedded in the middle was overlapping with the top surface (bottom in Fig. 3b), while the echo for the sensor at the deepest location was hardly separable from both surfaces' echoes (Fig. 3a). The echo in B-scans was used to extract the depth of sensor placement. The deepest sensor echo was sensed at 1 mm depth so considering the sensor

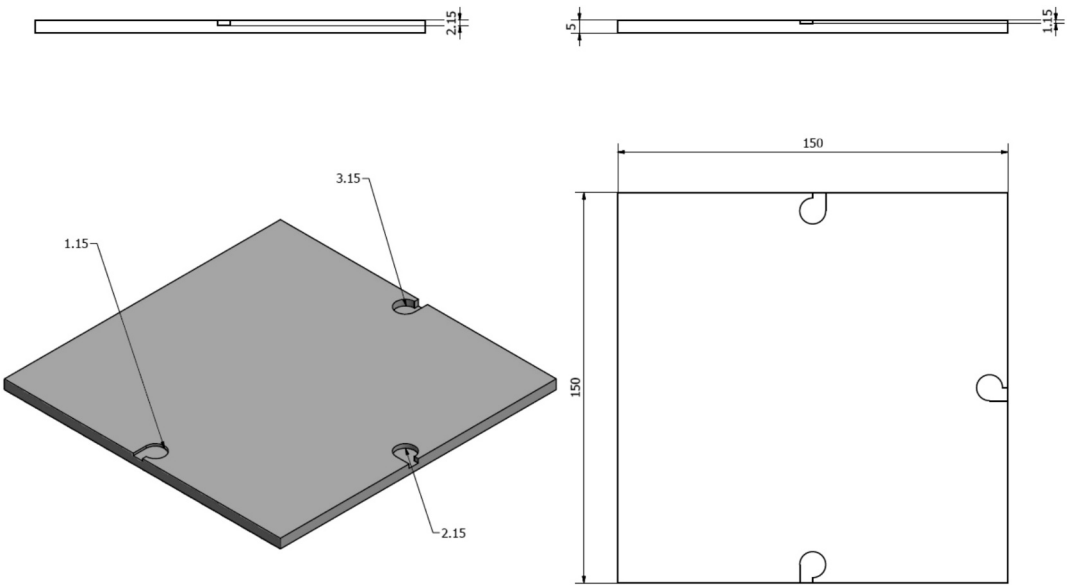

Fig. 1. Dimensions of the 3D printed sample with slots dedicated for sensors embedding.

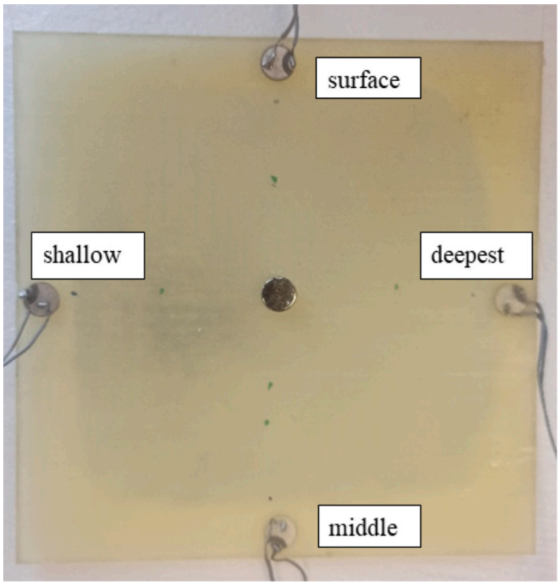

Fig. 2. The sample with surface bonded and embedded sensors. At the sample center there is a magnetic mass visible. The mass was used in the testing phase.

thickness (0.5 mm) and the plate thickness (5 mm) the depth of sensor placement was estimated at 3.5 mm. In the case the of middle sensor the echo was sensed from 1.87 mm resulting in a 2.63 mm depth of embedding. Finally, the shallow sensor was registered at 2.6 mm resulting in 1.9 mm depth of embedment. These readings confirm that, with good approximation, the sensors were embedded at the desired depths (1, 2, and 3 mm) and the depth was not affected significantly by the material filling process during the embedding.

All four sensors were employed for structural assessment of the plate using electromechanical impedance. However, the EMI study was preceded by wave propagation analysis as explained in the following section.

3. Scanning laser Doppler vibrometer-based analysis

The measurements and studies with the EMI were preceded by scanning laser Doppler vibrometer (SLDV) analysis. The EMI response is a frequency spectrum measured at the location of the piezoelectric sensor. It is not known what area of the sample is excited. If only part of the sample is excited the method will not be sensitive to structural changes located out of excitation region, so this research step was necessary to verify if the embedded sensors allow to excite the sample effectively. The SLDV measurements were conducted with a set-up as shown in *figure 3* of [32] (*https://ars.els-cdn.com/content/image/1-s2.0-S0888327023005538-gr3.jpg*), so the sample was hung freely by strings glued to its edges. For each measurement single sensor excited a tone burst signal comprising of 5 cycles with Hann modulation. The signal was generated by an arbitrary waveform generator (TTi TGA1241) and then amplified using a high-voltage amplifier (EPA-104 Piezo Linear Amplifier). A single SLDV laser head (Polytec PSV-400-3D) was used to measure the waves propagating in the plate by performing a full wavefield area scan in M=Nx × Ny = 10201 (Nx=Ny = 101) measurement points. The points were uniformly distributed horizontally and vertically with a 1.49 mm step. The measured wavefield indicate isotropic nature of the investigated sample. The wavefronts were circular showing the same wave propagation velocity irrespective of the direction.

The data gathered was next processed by calculating the normalized RMS (RMSn) value at each measurement point (i,j) for the time signals s with length K:

$$RMS(i,j) = \sqrt{\sum_{k=1}^{K} s_{ij}^2(k)} \tag{1}$$

$$RMSn(i,j) = \frac{RMS(i,j)}{\max_M\{RMS(i,j)\}} \tag{2}$$

where $\max_M\{\ \}$ designates a maximal value over all the measurement points M.

The sensors excitability was tested for three selected frequencies (35, 50, and 100 kHz) in order to determine the possibility to excite the sample with embedded sensors. The tests were not performed for frequencies above 100 kHz, because the measurements at 100 kHz showed that the wave is able to propagate throughout the sample only if it is excited by the surface bonded sensor (Fig. 4a). The sensor that is shallowly embedded excites only the region around it (Fig. 4b), while the measurements for deeper-placed sensors (middle, deepest) showed no wave propagation. Similarly, for 50 kHz excitation, only surface sensor is able to excite the wave propagating in the whole sample. Lowering the frequency to 35 kHz resulted in wave propagation observation for all the embedded sensors. The cases for which the wave propagation was visible throughout the sample are illustrated in Fig. 5 as an 1D intersection of the 2D RMSn images. The intersection was made along a line starting at the exciting sensor and ending on the opposite edge. So the left-hand side shows high values corresponding to the wave excitation and the values are dropping moving to the right-hand side due to attenuation of the wave in the material. At the end of the sample (distance = 150 mm) some oscillations can be observed that are related to wave reflecting from the edge and also interacting with the sensor that was placed there, as at each edge center there was one sensor. So, for example the wave propagating from a shallowly embedded sensor interacts with the deepest sensor (Fig. 2). Taking into consideration the observed wave behavior it was determined that the embedded sensors are not able to excite the sample effectively for higher frequencies, so it was decided to limit the EMI study up to 100 kHz.

Although the guided wave propagation is not the central point of this study the obtained result indicates that wave-based damage assessment techniques could encounter obstacles due to material attenuation in such printed polymer samples as the one investigated.

The excitation capability of embedded sensors at high frequencies could be enhanced by increasing the generation voltage and/or amplification. However, it would not help in the study of the

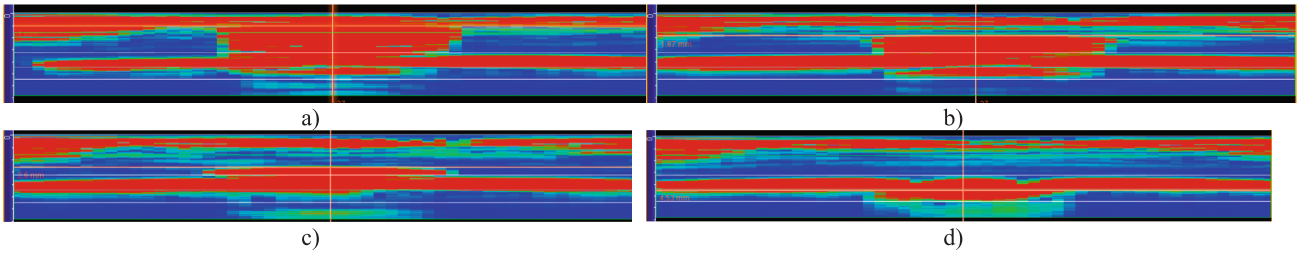

Fig. 3. Ultrasonic B-scan for 5 MHz frequency visualizing the sensor presence: (a) deepest sensor, (b) middle sensor, (c) shallow sensor, (d) surface bonded sensor.

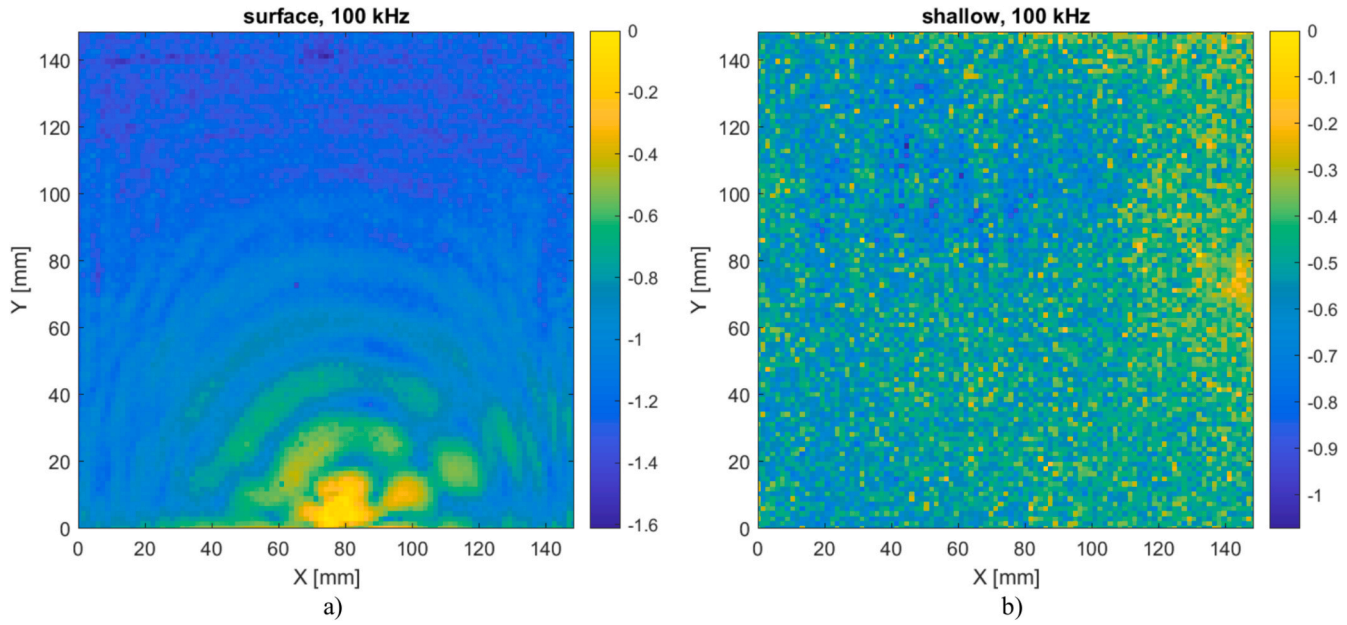

Fig. 4. Two dimensional (2D) visualization of the RMSn values for surface bonded (a) and shallowly embedded sensor (b). The colorbar is a logarithmic scale calculated as $\log_{10}$(RMSn) value, so the −1 value of the colorbar represents an RMSn value drop by 10 times with respect to the area near the sensors exciting the wave.

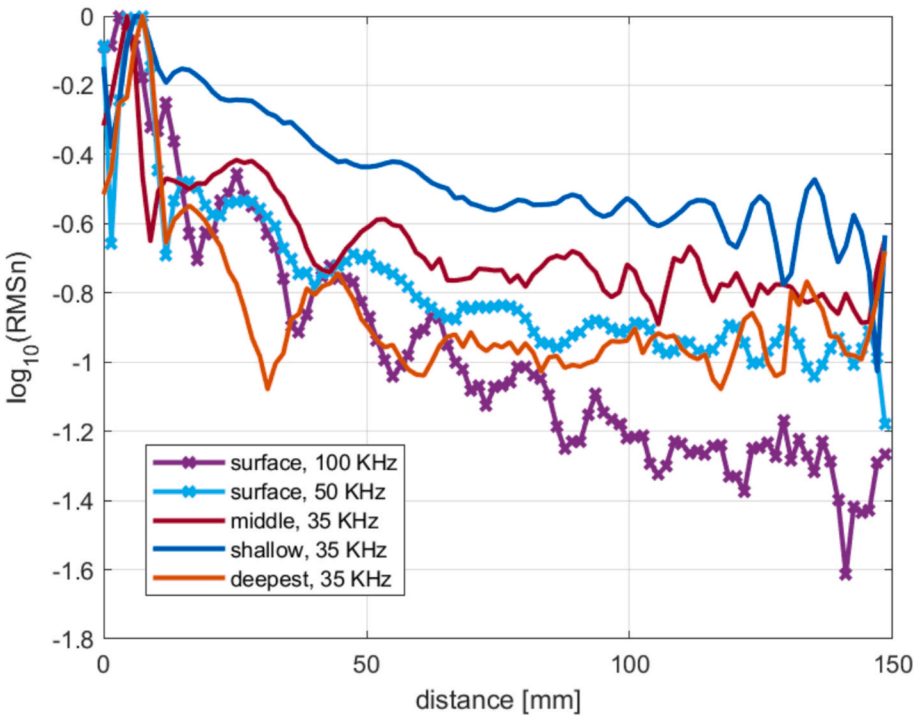

Fig. 5. The 1D values of normalized RMS for intersection of the 2D images (Fig. 4) along a line starting at the exciting sensor and ending on the opposite edge. The −1 value of y axis means a value drop of RMSn by 10 times.

electromechanical impedance, because the impedance analyzer was already used at the highest possible voltage for generation (next section) and amplification means were not available.

4. Electromechanical impedance study

The main aim of this research is to assess the possibility of EMI damage assessment using the embedded sensors. The SLDV study determined a frequency range limit of 100 kHz, so the EMI measurements were conducted in the range of 1 kHz to 100 kHz with fine 20 Hz step.

The EMI method is based on the measurements of electrical quantities of a piezoelectric transducer coupled (bonded, embedded) with the investigated structure. Due to electromechanical coupling of piezoelectric transducer and the host structure, mechanical resonances of structure can be observed in the electrical characteristics of the piezoelectric transducer. The coupled 1D electromechanical relationship was first introduced in [8] as:

$$Y(f) = i2\pi f a\left(\varepsilon^{T}(1-i\delta) - \frac{Z_{str}(f)}{Z_{str}(f)+Z_t(f)} d_{3x}^2 E\right) \quad (3)$$

where Y(f) is the electrical admittance of the piezoelectric element as a function of frequency (f). The i, a, ε^T, δ, d_{3x}, E are the imaginary unit, transducer geometric constant, zero stress dielectric constant, dielectric loss tangent, piezoelectric coupling constant, and complex Young's modulus of the transducer at the zero electric field, respectively. $Z_t(\omega)$ and $Z_{str}(\omega)$ are the mechanical impedance of the piezoelectric transducer and the plate, respectively.

In this research, the EMI measurements were made with a HIOKI IM 3570 impedance analyzer. Five volts is the excitation voltage chosen for the tests (the maximal value allowed by the device). An average of 50 measurements was taken during each test to improve the signal-to-noise ratio. All the measurements were conducted in stable room conditions. The measured quantities were the conductance (G), resistance (R), susceptance (B) and reactance (X) as a function of frequency. The measurements were divided into three rounds:

1. The first round comprised of two measurements of the sample healthy (undamaged) condition. These measurements were labeled as 'h1′ and 'h2′.
2. The second round comprised of three added mass cases for the simulation of changed mechanical state. A magnetic mass (10 mm in diameter and 2 g of weight on each side of the plate – Fig. 2) was added at three positions: 12 mm, 32 mm, and 68 mm away from the sensor edge. These three measurements were designated as 'close', 'medium' and 'far', respectively. This measurement was repeated for each of the four sensors.
3. The third round comprised of material removal by drilling. A through-thickness hole of 4 mm diameter was drilled at the center of the sample. Next the whole diameter was enlarged to 5, 6 and 7 mm. This round of measurements resulted in four cases labeled as '4 mm', '5 mm', '6 mm', and '7 mm'. This case represented local mass and stiffness change that could happen in reality due to impact.

The adding mass and drilling was chosen as a safer method of sample structural modification, that does not endanger the sensors. The impact damage or fatigue testing could cause sensor debonding, loose soldering or sensor damage. All of these would cause the change of the measured electrical quantities.

The whole measurement campaign resulted in 9 measurements for each sensor. As an example, Fig. 6 shows the raw conductance (G) signatures gathered in the first and second rounds of measurements for all the sensors. There are characteristic peaks visible in the curves and the curves differ slightly from each other. Although they have similar trend we do not see a clear difference between the response from each sensor. The other gathered responses (R, B, and X) also did not show a clear difference. The initial study reported in [31] showed that the RMSD index based on resistance can differentiate the added mass and detect the smallest hole (4 mm in diameter) presence. However, the studies conducted later did not showed a correlation of the RMSD index with the increase of the hole diameter. The same was observed for the conductance values, so there was a need to search for a new approach that allow for identification of the investigated cases.

Considering the capacitive nature of the piezoelectric sensor it is proposed here to use frequency dependent capacitance as a structural health sensitive feature. The frequency dependent capacitance C(f) can be calculated from susceptance (B). The susceptance is imaginary part of admittance given by Eq. (3). The frequency dependent capacitance is calculated from susceptance as [37]:

$$C(f) = \frac{B(f)}{2\pi f} \quad (4)$$

The obtained capacitance values for the measured cases are depicted in

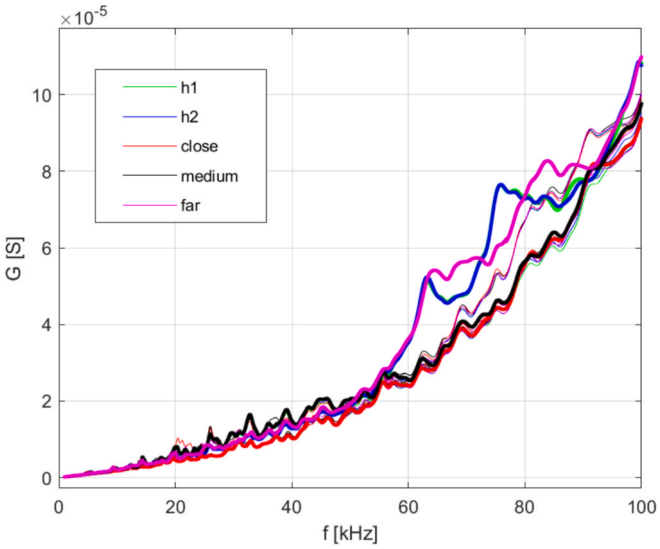

Fig. 6. Raw conductance signatures for healthy states (h1, h2) and added mass cases.

Fig. 7. The capacitance curve for a free sensor was also added for referential purposes. As it is seen, the capacitance for the free sensor has a value higher than for the surface-bonded sensor. This is in agreement with observations reported in [38] where the susceptance of the free sensor had the highest values in the frequency range up to 20 kHz, when compared to thermally bonded and glued sensors. The change of susceptance was also observed in the cited study due to impact causing sensor breakage, debonding and structural stiffness change. Since the capacitance is the frequency rescaled susceptance (Eq. (4), we observe here the same behavior up to in the 1 kHz –100 kHz range (Fig. 7). The values of the capacitance for embedded sensors drop even more. So, the deeper is the sensor the capacitance is lower. Based on the capacitance measurements it is easy to separate the responses from individual sensors, since adding a mass does not change the values significantly and four separate groups of curves are observed (Fig. 7a). However, the drilled holes measurements are not easily separated visually (Fig. 7b). Only the values for surface-bonded sensors are above the remaining cases. The capacitance for shallow and middle sensors overlap partially making it hard to distinguish them.

Due to the apparent segregation of the data according to the value of capacitance (Fig. 7) the mean value of capacitance together with standard deviation were calculated in the investigated frequency range from 1 kHz to 100 kHz. The standard deviation presents the capacitance variability in this frequency interval. The results are displayed in Fig. 8. In general, the mean capacitance value decreases as the depth of the sensor increases. The only exceptions are the 'close' and 'medium' added mass cases (Fig. 8a). Placing the mass close to the surface-bonded sensor makes the capacitance value comparable to the values for the deepest sensor, while for mass at the medium distance the capacitance value of surface-bonded sensor is similar to the values observed for the shallow sensor.

The mean values of capacitance can be used to distinguish the added mass cases for surface bonded sensor (Fig. 8a). The farther the mass is placed the capacitance value tends to the value observed for the healthy cases ('h1′ and 'h2′). This behavior is not observed for the remaining sensors. The study involving drilled holes (Fig. 8b) shows that even the surface-bonded sensor does not indicate sensitivity to the size of the hole. The capacitance value for the 7 mm hole is the most similar to the healthy cases, while the 5 mm hole value is the least similar. Also for the shallow, middle deepest sensors the capacitance for the 5 mm hole case is the lowest. These observations imply the need for a search of effective characteristics that can be related to the investigated structural change

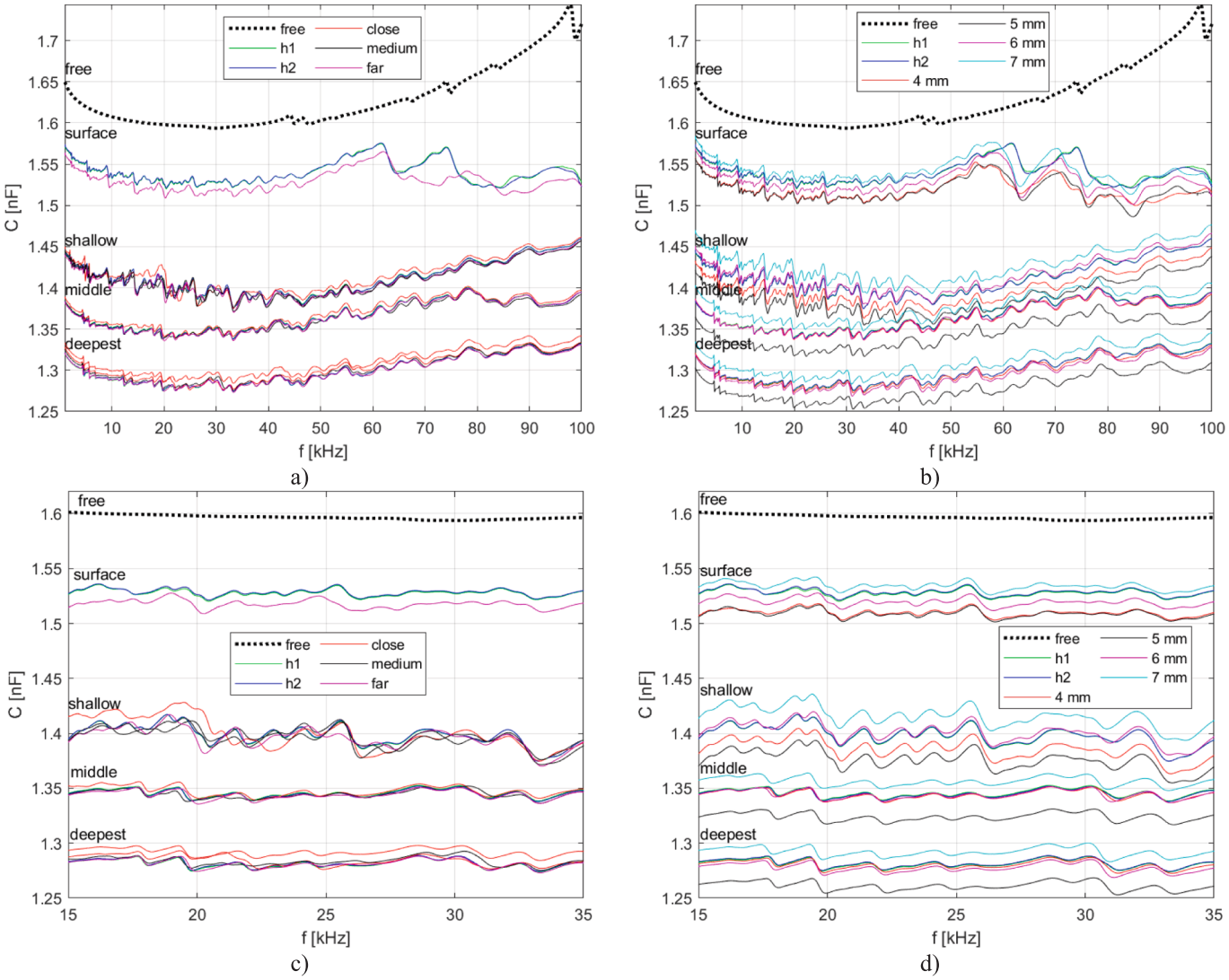

Fig. 7. Measured capacitance values of added mass cases (a) and drilled hole cases (b) compared with capacitance of free piezoelectric sensor in the 1–100 kHz frequency range; (c) added mass cases zoomed in 15–35 kHz range; (d) drilled hole cases zoomed in 15–35 kHz range.

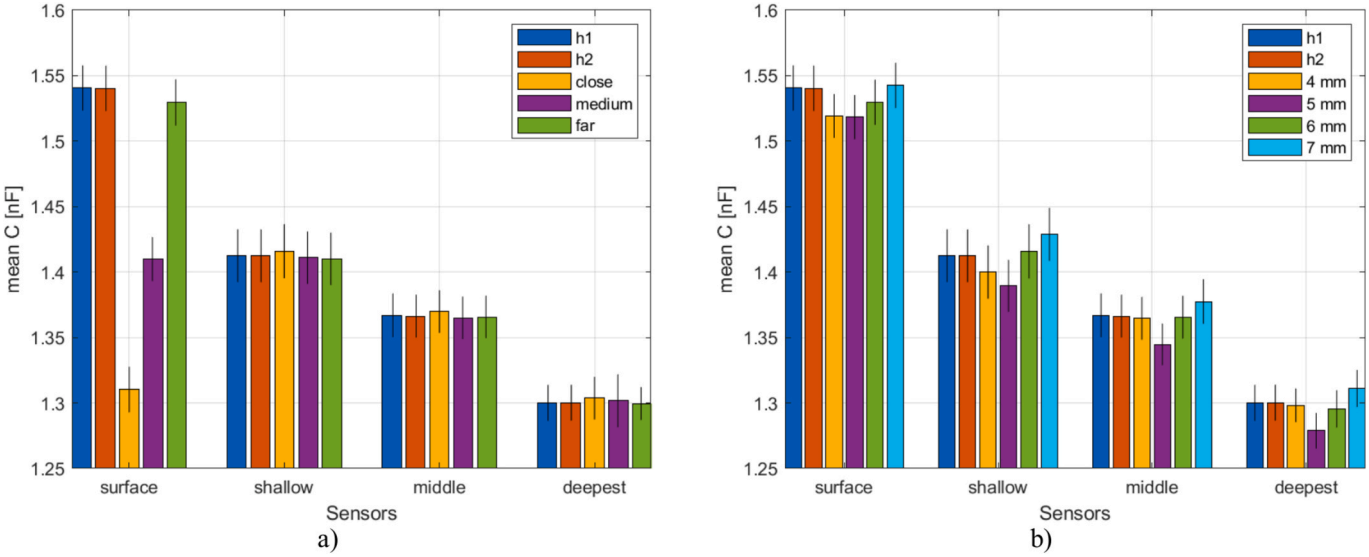

Fig. 8. The mean values of capacitance in the 1–100 kHz frequency range for all 4 sensors; a) added mass cases, b) drilled hole cases; the standard deviation is showing the variability of the capacitance in the frequency range.

severity (location of mass or size of the hole).

4.1. The influence of depth of the sensor placement on sensor capacitance

Although the mean capacitance value is not a good indicator of structural change, it can be used to distinguish the depth of the placement of sensors. Using the values of capacitance measurements for healthy cases ('h1′ and 'h2′) the value of mean capacitance with respect to the depth of sensor placement was investigated. The surface sensor depth was treated as zero and the shallow, middle, and deepest sensors were located at 1, 2, and 3 mm depths, respectively. Fig. 9a) depicts the four data points for the 'h1′ measurement with their standard deviation. The linear fit represents the data fairly well having R^2 equal to 0.95, while the cubic fit perfectly matches the data points and allows us to estimate the values for other depths thanks to the obtained cubic equation. The fitting coefficients were also calculated for the 'h2′ measurements. The linear fit has the same coefficients, while the cubic fit has only one different coefficient at x^2 equal to 0.092. Better linear fit is shown in Fig. 9b) for the case when the embedding depth obtained from ultrasonic B-scan is used (Fig. 3).

4.2. Structural change assessment based on capacitance

The shift of capacitance allowed to separate the responses from individual sensors but it is not helpful for structural state assessment. So the first step in processing is the remove the differences in the capacitance spectra (Fig. 7) caused by sensor embedding. The capacitance curves have a baseline shift. In the most simple cases it should be possible to remove the shift by subtracting the mean value. In the considered cases it was not enough and the shift could not be removed by just subtracting the mean value. So trend removal based on polynomial fit was applied. Polynomials were calculated that fits to the registered capacitance curves. The detrended capacitance vectors (Cd) were calculated as

$$Cd(f) = C(f) - P(f) \tag{5}$$

where the P(f) is the polynomial obtained using the *polyfit* function in MATLAB R2022a. The fit removed the horizontal shift effectively as it is seen in Fig. 10. However the fitting needed to be adjusted to the cases. Less variable added mass cases (Fig. 7c) where detrended with 5th degree polynomial resulting in curves seen in Fig. 10a). The data for the hole cases present larger variability (Fig. 7d) – the curves for the same sensor are distributed in larger capacitance range than for the added mass cases. Because of this, the more variable data for the drilled holes needed 20th degree polynomial (Fig. 10b).

Further, the detrended capacitance undergoes classification employing principal component analysis (*pca* function in MATLAB R2022a). Each capacitance vector is treated as an observation (W) and the capacitance value for given frequency is a variable (V). The data is arranged into a [Cdm] matrix

$$\left\{ \begin{array}{c} Cd_{h1}[1,2,\cdots,V] \\ Cd_{h2}[1,2,\cdots,V] \\ Cd_{close}[1,2,\cdots,V] \\ Cd_{medium}[1,2,\cdots,V] \\ Cd_{far}[1,2,\cdots,V] \end{array} \right\} \rightarrow [Cdm]_{V\times W} \tag{6}$$

Next, the covariance matrix [Cov] is created out of the [Cdm] matrix [25]:

$$[Cov]_{W\times W} = \frac{1}{V-1}[Cdm]^T[Cdm] \tag{7}$$

The eigenvectors of [Cov] matrix are sorted according to descending order of the eigenvalues. These vectors define the principal component space, so the first principal component is the vector corresponding to the highest eigenvalue, the second principal component corresponds to the second highest eigenvalue, and so on. Finally, the representation of the original data in the new space based on principal components that explains at least 95 % of the variance is analyzed to find differences between the healthy cases and the added mass cases. Exactly the same procedure is repeated for the Cd values for hole cases (Fig. 10b). For the added mass cases the 95.7 % of variance is explained by five principal components, while for the hole cases only four principal components are enough to explain 96.3 % of cases. Finally, the representation in the new space (denoted by superscript PC) is compared by calculating the Euclidean distance in the high dimensional principal component space between i-th case and the 'h1′ case

$$ED(i,h1) = \sqrt{\sum_{p=1}^{NPC}\left(\mathrm{Cd}_i^{PC}[p] - \mathrm{Cd}_{h1}^{PC}[p]\right)^2} \tag{8}$$

where the NPC = 5 for added mass cases and NPC = 4 for the hole cases. The results of ED calculations are depicted in Fig. 11, showing that the

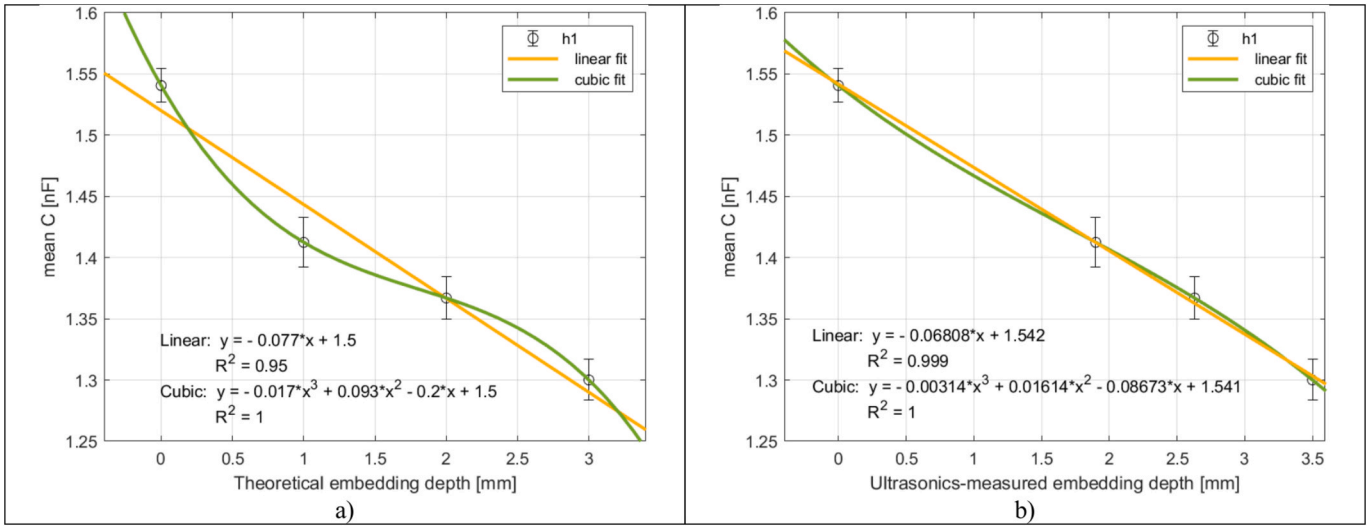

Fig. 9. The relation of the depth at which sensor is embedded and the calculated mean capacitance value; a) result for theoretical embedding depth, b) result for embedding depth obtained from ultrasonic B-scan; the plot shows linear and cubic fits.

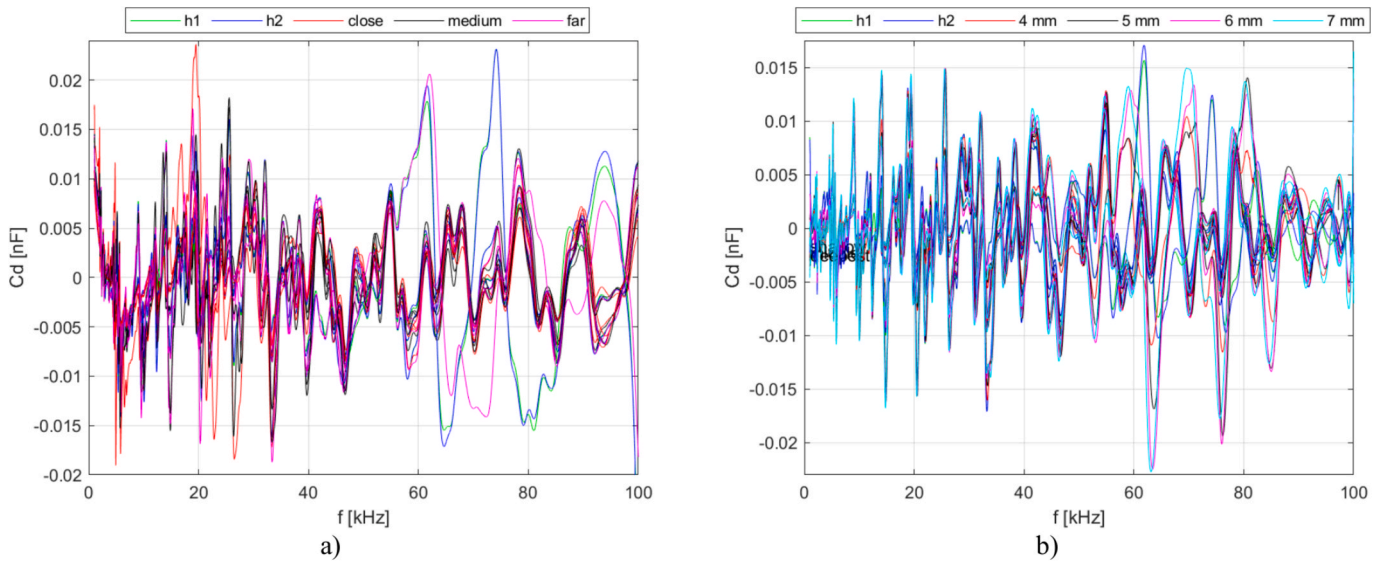

Fig. 10. Detrended capacitance curves using polynomial fitting; a) added mass cases, b) drilled hole cases.

ED values are a sensitive index. The value between the same cases is zero so the bar for 'h1′ is not visible. The difference between two healthy cases ('h1′ and 'h2′) is marginal for all the sensors and cases. The farther the mass is from the sensor the more ED value decreases (Fig. 11a). This is observed for all the sensors. There is a clear difference in sensitivity to the mass depending on the sensor depth. The surface-bonded sensor is characterized by a moderate drop in the ED values when the mass is moved farther away from the sensors. Meanwhile, the other sensors show low ED values for the mass placed farthest. The results for the second set of data show that the larger the hole diameter is, the ED value is larger (Fig. 11b). This is not observed when RMSD index is used for resistance or conductance (Fig. 12). The RMSD was calculated with respect to 'h1′ measurement, similarly as for ED values in Fig. 11. The RMSD value is fluctuating and is not growing with the increase of the hole diameter. In previously published study, the RMSD was only sensitive to the additional mass [31]. The other popular EMI index is the mean absolute percentage deviation (MAPD) index. It was also tested for resistance and conductance spectra and is not showing the wanted sensitivity to increasing hole diameter.

The drop of the ED values for embedded sensors are significant with respect to the surface-bonded sensor result. Table 1 shows the relative ED values in percentage. The ED values for the shallow, middle and deepest sensor are below 50 % for all the analyzed cases. The relation of the depth of sensor embedding and structural features shows that the highest sensitivity (47.3 %) is obtained only for shallowly embedded sensor when the additional mass is close to the sensor. Also, if the mass is close to the sensor, the ED value indicates more sensitivity – the ED value increase for the deepest sensor, while for the medium and far placed mass the value decreases as the depth of the sensor increases. Another important observation is that the ED value behave differently for the added mass cases and the drilled hole cases. The ED value for drilled hole increases for the middle sensor (Table 1) and then drops for the deepest sensor. This is not observed for the added mass cases. This indicates better sensitivity of the middle sensor if the structural change/defect is through thickness (hole) not only on the surface (mass). The former research in the reinforced concrete monitoring showed that the way of sensor integration with the monitored structure plays important role in the sensitivity of the EMI method [14]. The monitoring efficiency

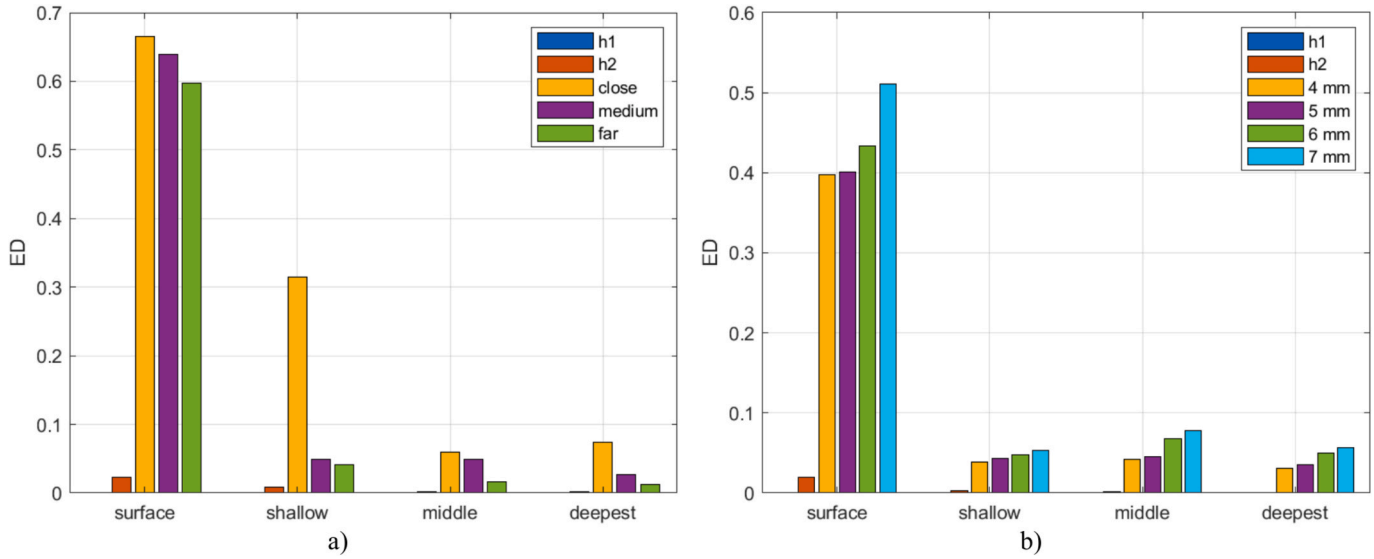

Fig. 11. Euclidean distance calculated in the principal component space and used as damage index to differentiate the investigated cases of: (a) additional mass, (b) through thickness hole.

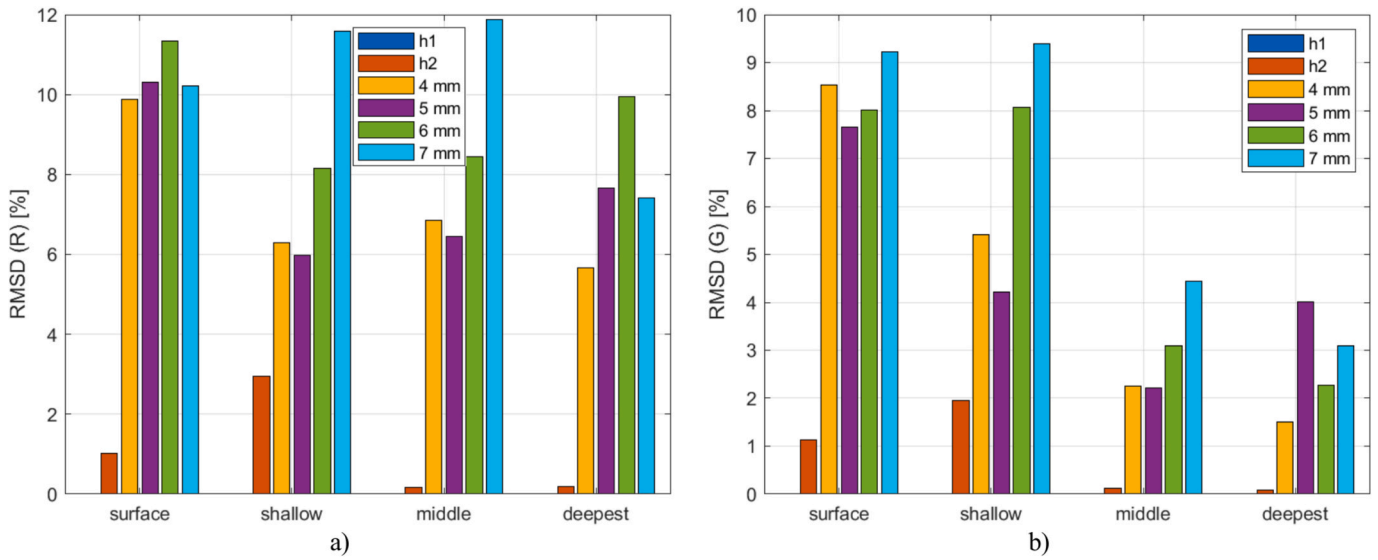

Fig. 12. RMSD index value calculated for the hole cases for a) resistance, (b) conductance in the 1 kHz-100 kHz range.

Table 1
The relation of the depth of sensor embedding and relative ED values in relation to the surface bonded sensor result.

		Case						
		Added mass cases			Hole cases			
		close	medium	far	4 mm	5 mm	6 mm	7 mm
Depth	*surface*	100.0 %	100.0 %	100.0 %	100.0 %	100.0 %	100.0 %	100.0 %
	shallow	47.3 %	7.8 %	6.9 %	9.7 %	10.8 %	11.1 %	10.4 %
	middle	8.9 %	7.8 %	2.8 %	10.6 %	11.2 %	15.6 %	15.3 %
	deepest	11.2 %	4.2 %	2.1 %	7.7 %	8.8 %	11.5 %	11.1 %

was inseparably linked with sensor positioning to the examined host structure. Here the dependence of the damage sensitivity on the depth of embedding was observed.

5. Conclusions

The study reported here uses frequency-dependent capacitance of piezoelectric sensors as a structural health sensitive feature. The study allowed to establish the relation between the depth of sensor embedding and capacitance mean value.

New data processing was introduced for damage assessment. The trend from capacitance spectra is removed by employing a polynomial fit. The principal component analysis rearranges the data and reduces the number of investigated variables. The Euclidean distance in the new space serves as a damage index successfully differentiating all the investigated cases. The study showed that the structural damage assessment using EMI can be realized by embedded sensors but their sensitivity is lower than for the surface-bonded sensor. In practical application the lower range of sensitivity of embedded sensors means that more sensors need to be used and the inspection of larger structural parts would require a dedicated sensor network. So for a sensor network the embedded sensors need to be more closely spaced in comparison to surface-mounted sensors. The inspection of larger areas should be possible then by taking the proposed approach based on capacitance and applying it individually to each sensor of the network. Next the individual responses should be fused as other authors did in previously published works [28,30]. The range of single sensor could possibly be extended by seeking methods of amplification of the impedance analyzer excitation signals. Also, the optimal depth of embedment need to be determined individually depending on the structure. So the sensors in a network would be placed in spacing that allows for detection depending on the sensor sensitivity range.

The structural assessment was successfully made in a relatively low frequency range (below 100 kHz). This is an important advantage, since many researchers use low-cost EMI solutions based on Analog Devices AD5933 chip that works only up to 100 kHz [39]. The studies were made in stable room conditions, so the temperature was not a parameter of the study here. However, the variability of the temperature should not influence the applicability of the method. Recent EMI temperature study in the −15 °C to 45 °C range showed that the conductance peak frequency and amplitude exhibit noticeable variations with temperature [40]. As the temperature increases, the resonance peaks shift leftward, indicating a decrease in resonance frequency. The conductance magnitude increases with the temperature. So, either the temperature inference can be compensated [41] or there is a need to have a set of referential measurements for various temperatures. Depending on the temperature during new measurement, it should be compared against the reference data collected at the corresponding temperature.

Future studies should consider more realistic damage cases. But for this an effective method of sensor protection needs to be developed. Also, thicker samples should be analyzed to allow for even more depths to be investigated to confirm the observed relationship between the mean capacitance value and the depth of sensor embedding. The data processing approach worked effectively for the two cases studied (added mass and drilled holes). No adjustment was needed. If other material and damage type is taken we can assume that the signal processing would work if the EMI is sensitive to this damage and the damage is within the sensor sensitivity range.

CRediT authorship contribution statement

Paweł H. Malinowski: Writing – review & editing,

Conceptualization, Methodology, Validation, Formal analysis, Investigation, Visualisation, Funding acquisition, Resources, Supervision. **Artur Andrearczyk:** Resources, Visualisation, Writing – review & editing, Methodology, Investigation. **Shishir Kumar Singh:** Conceptualization, Methodology, Investigation, Writing – review & editing.

Declaration of competing interest

The authors declare that they have no known competing financial interests or personal relationships that could have appeared to influence the work reported in this paper.

Acknowledgments

The authors acknowledge the funding support provided by the National Science Center, Poland under the OPUS project entitled: Health monitoring of ADditively manufactured structurES (HADES) (2019/35/B/ST8/00691).

Data availability

Data will be made available on request.

References

[1] T.D. Ngo, A. Kashani, G. Imbalzano, K.T. Nguyen, D. Hui, Additive manufacturing (3D printing): a review of materials, methods, applications and challenges, Compos. B Eng. 143 (2018) 172–196.
[2] F. Le Bourdais, et al., On the potential of Resonant Ultrasound Spectroscopy applied to the non-destructive characterization of the density of (LPBF) additively manufactured materials, Addit. Manuf. 58 (2022) 103037.
[3] Y. Jin, E. Walker, H. Heo, A. Krokhin, T.-Y. Choi, A. Neogi, Nondestructive ultrasonic evaluation of fused deposition modeling based additively manufactured 3D-printed structures, Smart Mater. Struct. 29 (4) (2020) 045020.
[4] M.O. Öteyaka, F.H. Çakir, M.A. Sofuoğlu, Effect of infill pattern and ratio on the flexural and vibration damping characteristics of FDM printed PLA specimens, Mater. Today Commun. 33 (2022) 104912.
[5] N. Kizer, C.M. Kube, In situ monitoring of polymer 3D printing using ultrasonic Lamb waves generated by a 3D printed wedge, J. Acoust. Soc. Am. 150 (4) (2021) A308–A.
[6] B.S. Vien, W.K. Chiu, L.F. Rose, Experimental investigation of second-harmonic lamb wave generation in additively manufactured aluminum. J. Nondestruct. Evaluat., Diagnost. Prognost, Eng. Syst. 1 (4) (2018).
[7] E. Brun, E. Dos Santos, G. Rival, P.J. Cottinet, A. Pelletier, B. Ducharne, Printed ultrasound sensors for enhanced structural health monitoring: development, characterization, and real-time evaluation, Smart Materials and Structures (2025), https://doi.org/10.1088/1361-665X/adb4b3.
[8] C. Liang, F.P. Sun, C.A. Rogers, Coupled electro-mechanical analysis of adaptive material system—determination of the actuator power consumption and system energy transfer, J. Intell. Mater. Syst. Struct. 5 (1994) 12–20.
[9] S. Zhao, S. Fan, J. Yang, S. Kitipornchai, Numerical and experimental investigation of electro-mechanical impedance based concrete quantitative damage assessment, Smart Mater. Struct. 29 (5) (2020) 055025.
[10] S. Zhao, S. Fan, J. Yang, S. Kitipornchai, A spherical smart aggregate sensorbased electro-mechanical impedance method for quantitative damage evaluation of concrete, Struct. Health Monit. 19 (5) (2019) 1560–1576.
[11] R. Perera, L. Torres, A. Ruiz, C. Barris, M. Baena, An EMI-based clustering for structural health monitoring of NSM FRP strengthening systems, Sensors 19 (2019) 3775.
[12] R. Sun, E. Sevillano, R. Perera, Debonding detection of FRP strengthened concrete beams by using impedance measurements and an ensemble PSO adaptive spectral model, Compos. Struct. 125 (2015) 374–387.
[13] D. Ai, H. Luo, H. Zhu, Numerical and experimental investigation of flexural performance on pre-stressed concrete structures using electromechanical admittance, Mech. Syst. Sig. Process. 128 (2019) (2019) 244–265.
[14] M.C. Naoum, N.A. Papadopoulos, G.M. Sapidis, M.E. Voutetaki, Efficacy of PZT Sensors Network Different Configurations in Damage Detection of Fiber-Reinforced Concrete Prisms under Repeated Loading, Sensors 24 (17) (2024) 5660.
[15] N.-L. Dang, Q.-Q. Pham, J.-T. Kim, Piezoelectric-based hoop-type interface for impedance monitoring of local strand breakage in prestressed multi-strand anchorage, Struct. Control Health Monit. 28 (2021) e2649.
[16] G.M. Sapidis, M.C. Naoum, N.A. Papadopoulos, Electromechanical Impedance-based Compressive Load-Induced damage Identification of Fiber-Reinforced Concrete, Infrastructures 10, no. 3 (2025) 60.
[17] S.K. Singh, M.A. Fakih, Mustapha, P.H. Malinowski, Damage Sensitivity Study in 3D-printed PLA of Different Infill Densities using the Electromechanical Impedance Method. Proceedings of the Fourteenth International Workshop on Structural Health Monitoring (IWSHM), 2023.
[18] M.I. Albakri, L.D. Sturm, C.B. Williams, P.A. Tarazaga, Impedance-based non-destructive evaluation of additively manufactured parts, Rapid Prototyp. J. 23 (3) (2017) 589–601.
[19] F.H. Çakır, Ü. Er, M. Tekkalmaz, M.A. Sofuoğlu, Evaluation of electromechanical impedance, modal and X-ray testing as non-destructive methods for additively manufactured plastics, Nondestr.Test. Eval. (2025) 1–26.
[20] I.T. Jolliffe, Principal Component Analysis, Springer Ser. Statist. (1986).
[21] S. Park, J. Lee, C. Yun, D.J. Inman, Electro-Mechanical Impedance-based Wireless Structural Health monitoring using PCA-Data Compression and k-means Clustering Algorithms, J. Intell. Mater. Syst. Struct. 19 (4) (2008) 509–520.
[22] H.J. Lim, M.K. Kim, H. Sohn, C.Y. Park, Impedance-based damage detection under varying temperature and loading conditions, NDT&E Int. 44 (2011) 740–750.
[23] P. Selva, O. Cherrier, V. Budinger, F. Lachaud, J. Morlier, Smart monitoring of aeronautical composites plates based on electromechanical impedance measurements and artificial neural networks, Eng. Struct. 56 (2013) 794–804.
[24] J. Min, J.-H. Yi, C.-B. Yun, Electromechanical impedance-based long-term SHM for jacket-type tidal current power plant structure, Smart Struct. Syst. 15 (2) (2015) 283–297.
[25] T.-C. Huynh, N.-L. Dang, J.-T. Kim, PCA-based filtering of temperature effect on impedance monitoring in prestressed tendon anchorage, Smart Struct. Syst. 22 (1) (2018) 57–70.
[26] A.G. Scheyer, S.R. Anton, Impedance-Based Structural Health Monitoring of Additive Manufactured Structures with Embedded Piezoelectric Wafers Vol. 10168 (2017) 616–625.
[27] X.P. Qing, S.J. Beard, A. Kumar, T.K. Ooi, F.K. Chang, Built-in sensor network for structural health monitoring of composite structure, J. Intell. Mater. Syst. Struct. 18 (1) (2007) 39–49.
[28] J. Zhu, X. Qing, X. Liu, Y. Wang, Electromechanical impedance-based damage localization with novel signatures extraction methodology and modified probability-weighted algorithm, Mech. Syst. Sig. Process. 146 (2021) 107001.
[29] C. Kralovec, M. Schagerl, M. Mayr, Localization of damages by model-based evaluation of electro-mechanical impedance measurements, in: Proceedings of the 9th EWSHM, 2018, pp. 10–13.
[30] S.K. Singh, R.N. Soman, P.H. Malinowski, A novel multi-damage localization method for polymers and composites based on electromechanical impedance, Mech. Syst. Sig. Process. 216 (2024) 111508.
[31] S.K. Singh, A. Andrearczyk, P.H. Malinowski, Damage Detection in 3D-Printed Plate Using the Electromechanical Impedance Method with Surface Bonded and Embedded Sensors Vol. 12951 (2024) 195–200.
[32] M.A. Fakih, S.K. Singh, S. Mustapha, M. Radzienski, P.H. Malinowski, A comprehensive analysis of guided-wave propagation in 3D-printed PLA plates with different infill densities–Experimental study, Mech. Syst. Sig. Process. 202 (2023) 110645.
[33] Q.-B. Ta, Q.-Q. Pham, N.-L. Pham, T.-C. Huynh, J.-T. Kim, Smart Aggregate-based Concrete stress monitoring via 1D CNN Deep Learning of Raw Impedance Signals, Struct. Control Health Monit. 5822653 (2024).
[34] C.K. Soh, K.-K.-H. Tseng, S. Bhalla, A. Gupta, Performance of smart piezoceramic patches in health monitoring of a RC bridge, Smart Mater. Struct. 9 (4) (2000) 533–542.
[35] R. Gomasa, V. Talakokula, S.K.R. Jyosyula, T. Bansal, Strength monitoring and Prediction of Blended Concrete Systems from very Early to delayed Age using embedded Piezo Sensor Data: an Experimental and Machine Learning Approach, Journal of Building Engineering 112677 (2025).
[36] https://www.ceramtec-group.com/fileadmin/user_upload/Corporate/11_Downloads/04_Piezo_Ceramics/Datasheet_Piezo_Soft_Materials_EN.PDF (accessed on 9th of April, 2025).
[37] https://www.electronics-tutorials.ws/accircuits/parallel-resonance.html (accessed on 9th of April, 2025).
[38] S. Park, G. Park, C.B. Yun, C.R. Farrar, Sensor self-diagnosis using a modified impedance model for active sensing-based structural health monitoring, Struct. Health Monit. 8 (1) (2009) 71–82.
[39] A. Zagrai, A. Misla, J. Sanchez, D. Powell, Electro-Mechanical Impedance Method for Structural Health monitoring of Space Structures: from Laboratory Experiments to Measurements during Spaceflight, in: AIAA Propulsion and Energy 2020 Forum, 2020, https://doi.org/10.2514/6.2020-3529.
[40] Mirgal, P., del-Río-Velilla, D., Wandowski, T., Majewska, K., and Malinowski, P. H. (2025, May). Temperature-driven changes in electromechanical impedance technique applied for damage detection in 3D printed plates. In Health Monitoring of Structural and Biological Systems XIX (Vol. 13437, pp. 287-292). SPIE.
[41] X. Huang, Q. Wenzhong, X. Li, Temperature compensation method for impedance signals of bolt loosening under temperature varying conditions using TransUnet, Smart Mater. Struct. 33 (10) (2024) 105035.